Microfluid Nanofluid (2010) 9:385–396
DOI 10.1007/s10404-009-0556-9

RESEARCH PAPER

A dynamic piezoelectric micropumping phenomenon

M. Yakut Ali · Cuifang Kuang · Jamil Khan · Guiren Wang

Received: 15 August 2009 / Accepted: 3 December 2009 / Published online: 24 December 2009

Abstract A dynamic micropumping phenomenon has been observed, which is based on acoustic streaming generated by a piezotransducer actuated in d_{31} mode without check valve. The use of d_{31} mode of a piezoelectric microtransducer can significantly enhance the pumping performance for application in miniaturization. Experimental study of the maximum local velocity has been conducted to investigate the effect of actuator tip configuration on the micropumping performance. In addition, this study also shows the quantitative measurement of the pumping performance such as the pressure head generated as a function of different relevant parameters like applied electrical field, AC frequency, and length of the actuator.

Keywords Dynamic micropumping · Acoustic streaming · Piezoelectric microtransducer · d_{31} mode · Miniaturization · Actuator tip configuration

1 Introduction

Recent progress in microfluidics or lab-on-a-chip devices has shown its revolutionary impact in chemical and biological assays (Beebe et al. 2002; Reyes et al. 2002). Micropumps are the essential components in microfluidic system (Kan et al. 2008).

M. Yakut Ali · C. Kuang · J. Khan
Department of Mechanical Engineering, University of South Carolina, Columbia, SC 29208, USA

G. Wang (✉)
Department of Mechanical Engineering & Biomedical Engineering Program, University of South Carolina, Columbia, SC 29208, USA
e-mail: guirenwang@sc.edu

A significant number of experimental and computational research efforts have been made for the last 30 years to develop innovative micropumping technology with application to diverse areas which include, but not limited to the microfluidic systems. The research effort continues as the specific requirement of a micropump for a particular application varies from one to another and poses several design and fabrication challenges. In Bio-Engineering, several micropumps have been developed for transdermal drug delivery (Ma et al. 2006), controlled drug delivery (Cui et al. 2007), breaking and removing blood clot in the brain, i.e., blood pumping (Wang et al. 2004), local delivery of basic fibroblast growth factor (bFGF) over a specific dose, and time course for tissue regeneration (Ryu et al. 2007). Another potential and attractive application field of micropumping technologies may be the space exploration (Laser and Santiago 2004).

Unconventional and innovative micropumping technologies are also considered as alternative for single- and two-phase cooling of microelectronics devices where increased power density and tendency to miniaturization demand smaller equipment with lower noise generation and power consumption (Singhal et al. 2004). Another consideration in microelectronics cooling area has been the integration of micropump into microchannel heat sink, and thus essentially elimination of a system component, i.e., the external pump in this case (Garimella et al. 2006). Microelectronics cooling demands higher flow rate, so that high heat fluxes may be handled, while minimizing temperature gradients on the chip. Recent studies indicate that two-phase convective cooling of a 100 W microchip would require flow rates of order 10 ml min^{-1} or more (Zhang et al. 2002).

Comprehensive and extensive reviews of past and recent research activities relating to principles, characteristics, materials, fabrication technology, and performance

characterization parameters of micropumps have been presented by several authors (Laser and Santiago 2004; Woias 2005; Zhang et al. 2007; Iverson and Garimella 2008). Micropumps generally fall into one of two major categories according to the classification presented by Laser and Santiago (2004): (1) displacement pumps, which exert pressure forces on the working fluid through one or more moving boundaries and (2) dynamic pumps, which continuously add energy to the working fluid in a manner that increases either its momentum or its pressure directly. The first group includes the so-called reciprocating micropumps that use the oscillatory or rotational movement of mechanical parts to displace fluid, the most known of which are the diaphragm pumps. In the other group (dynamic pumps), centrifugal, electrohydrodynamics, electroosmotics, magnetohydrodynamics, acoustic streaming, ultrasonic, and other types of pumps are found. Reciprocating micropumps are generally suitable for the delivery of all gaseous and low viscosity fluids and most but not all dynamic pumps depend on certain properties of the fluid such as ionic strength.

A wide variety of actuation schemes, such as piezoelectric (Koch et al. 1998a, b), electrostatics (Bourouina et al. 1997), magnetic (Ahn and Allen 1995), thermal (Tsai and Lin 2002), thermopneumatic (Jeong and Yang 2000), electromagnetic (Gong et al. 2000) actuation, and ultrasonic flexural plate wave (Nguyen and White 1999) have been adopted to develop micropumps. Many of recently developed flow pumps are based on the use of piezoelectric actuators that have relatively simple structure, high output power density, precise metering ability, less power consumption, capability of system integration, and more importantly ease of miniaturization. For example, a piezoelectric pump is the diaphragm pump, which, in principle, is similar to a piston pump. This pump uses a piezoelectric actuator to move a membrane in a chamber providing fluid entrance and exit with the flow direction being controlled by check valves which have been investigated by many researchers (Koch et al. 1998a, b; Ullman et al. 2001).

Several valveless displacement dynamic micropumps have also been reported in literature (Cui et al. 2007; Koch et al. 1998a, b; Gerlach et al. 1995). The operational principle is based on the motion of the piezoelectrically actuated pump membrane and flow rectifying properties of the diffuser/nozzle element or truncated pyramid-shaped microchannels to mimic the operation of check valves. A flow pump using bimorph piezoelectric actuator to generate flow in both liquid (Lima et al. 2009) and air has been investigated by several researchers (Acikalin et al. 2004; Basak et al. 2005; Kim et al. 2004). On the other hand, several studies have been published on generating acoustic streaming flow using piezoelectric actuator or other transducers (Hashimoto et al. 1997; Rife et al. 2000) as well. Acoustic streaming theory has been discussed in detail by Nyborg (1998). Hashimoto et al. (1997) proposed the application of acoustic streaming to develop micromanipulators for small particles using a two-dimensional ultrasonic transducer array as ultrasonic waves induce acoustic streaming very efficiently only in the vicinity of the transducer. They concluded that micropumps can also be developed by combining a transducer array with a topographic channel structure for liquid flow. Rife et al. 2000 demonstrated the miniature acousto-fluidic devices which could find application in pumping in low impedance planar and closed loop systems and also for mixing in low Reynolds number flows based on acoustic attenuation exerted on fluid by exciting the piezotransducers at radio frequency. The application of acoustic streaming induced by ultrasonic flexural vibrations for enhancement of convective heat transfer has also been reported (Loh et al. 2002). Recently, surface acoustic wave (SAW) induced streaming and pumping have been reported for microfluidics applications as well (Du et al. 2009).

The present study aims at the study and experimental characterization of a novel dynamic micropumping phenomenon using a micropiezotransducer in d_{31} mode having no check valve. In the present configuration, a single oscillating piezoelectric transducer is placed in a fluid (water) to generate flow. To the best of our knowledge, no flow pumping phenomenon has been reported so far based on the so-called d_{31} actuation mode (which will be discussed in details in the following paragraph) of a piezoelectric transducer. In this article, we demonstrate experimentally the pumping performance of the single piezotransducer-actuated pump without valves. The pumping effect is based on acoustic steady streaming resulting from oscillation of a piezotransducer. Experimental study has been conducted to present the effect of actuator tip configuration and some other parameters on pumping performance. The pumping phenomenon demonstrated falls in the category of dynamic pump as defined by Laser and Santiago (2004). The corresponding pumping with only one micropiezotransducer can provide flow rates in excess of 0.2 ml min^{-1} and maximum pressure heads of about 11 mm of H_2O. This study also provides experimental data for future modeling efforts.

2 Piezoelectric actuator: principle and transducer selection

A simplified description based on piezoelectric theory can be used to guide the selection of the single transducer. The displacement of a single piezoelectric transducer can be mathematically described as follows (Askeland and Phule 2006):

$$\delta_l = d_{ij} l_0 E = d_{ij} l_0 \frac{V}{D_f} \quad (1)$$

where δ_l, d_{ij}, l_0, E, V, and D_f are the displacement, piezoelectric coefficient tensor, original length of the transducer without electrical field, applied electrical field, applied electrical voltage, and the electrode separation distance, respectively. Note that the displacement of the transducer is proportional to its original length and piezoelectric coefficient, applied voltage, and is inversely proportional to distance between the two electrodes. In order to generate high flow velocity with voltage as low as possible (i.e., consume electric power as less as possible), it is expected that the displacement of the piezoelectric transducer should be maximized at a given frequency.

The piezoelectric coefficient tensor is determined by the intrinsic physical properties of the piezoelectric transducer. Of particular importance are the so-called d_{33} and d_{31} components of the piezoelectric coefficient tensor. In the d_{33} mode of vibration, the displacement direction is aligned with the electric field, whereas the electric field is orthogonal to the vibration direction for the d_{31} mode as shown in Fig. 1a and b. Typically, piezoelectric coefficient d_{33} is 2–4 times larger than d_{31}. Therefore, apparently it seems to be more efficient to use d_{33} mode than to use d_{31} mode of vibration assuming that the other parameters in Eq. 1 are the same in both cases. However, the flow velocity of acoustic streaming increases with the increase of δ_l. It is clear from Fig. 1a that l_0 and D_f in Eq. 1 are the same in d_{33} mode. Therefore, in this mode, for a particular length of piezotransducer and for a given voltage, the displacement δ_l is proportional to d_{33} and V. On the other hand, for d_{31} mode, l_0 can be much larger than D_f and thus δ_l can be several order higher in d_{31} mode than in d_{33} mode. Thus, d_{31} mode is selected for this study. The dynamic micropumping phenomenon observed in this study is due to acoustic streaming generated by the piezotransducer. Sound wave generated by the transducer in d_{31} mode will travel through the liquid and pass the energy to liquid to induce the streaming.

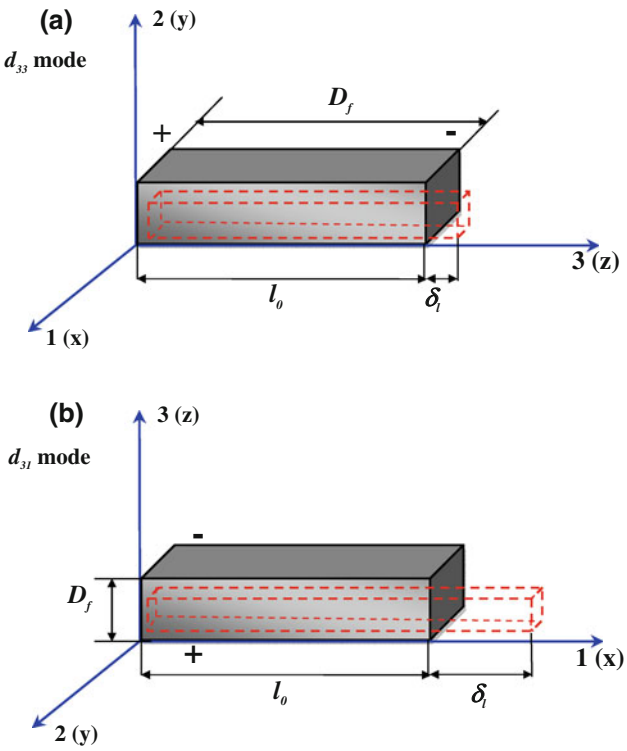

Fig. 1 d_{33} and d_{31} modes of actuation of a piezoelectric transducer. **a**: d_{33} mode; **b**: d_{31} mode

3 Experimental setup and actuator configuration

3.1 Experimental setup and measurements

Figure 2a shows the experimental setup used for the flow experiments. The experiments were performed in a plexiglass rectangular reservoir of size 60 × 40 × 20 mm^3, filled with deionized (DI) water as working fluid. A micropiezotransducer PZT 5A3 from Smart Material Corp. (with rectangular cross-section of 360 μm × 260 μm) was selected as the actuator, since it would give more flexibility and chance of miniaturization. Different transducer lengths (30, 20, 14.4, and 10 mm) with the same cross-sectional area were used to investigate the effect of length on the pumping performance. Thin copper wires were connected to the piezoactuator for applying external electrical field. A homemade liquid dip coating system was used for uniform coating of the piezoactuator which would work as electric insulator and thus prevent from forming bubbles when it is immersed in water. Polyurethane was used as coating fluid. After coating the dimensions of the transducer became 600 μm × 580 μm. Pinhole free-coated entire piezoactuator was then inserted into the plexiglass rectangular reservoir through a hemostasis valve from Qosina Corporation (Edgewood, NY) which was connected to the sidewall of the reservoir, and the connection was sealed with an O-ring. The hemostasis was used to seal the electric wires that were connected to the peizotransducer. Inside the reservoir, the piezoelectric actuator was placed coaxially to a glass tube with 1 mm inner diameter (ID) and a 90° turn at one end. The relative position between the tube end and transducer tip in this setup can be adjusted by a 3D micropositioning stage. Note that the piezotransducer is fixed in the reservoir, and the tube with 90° turn is not permanently attached to the transducer. A dual channel function generator AFG 3102 from Tektronix in combination with a KH 7602M amplifier from Krohn-Hite Corporation was used to provide the required external electrical field to the piezoactuator.

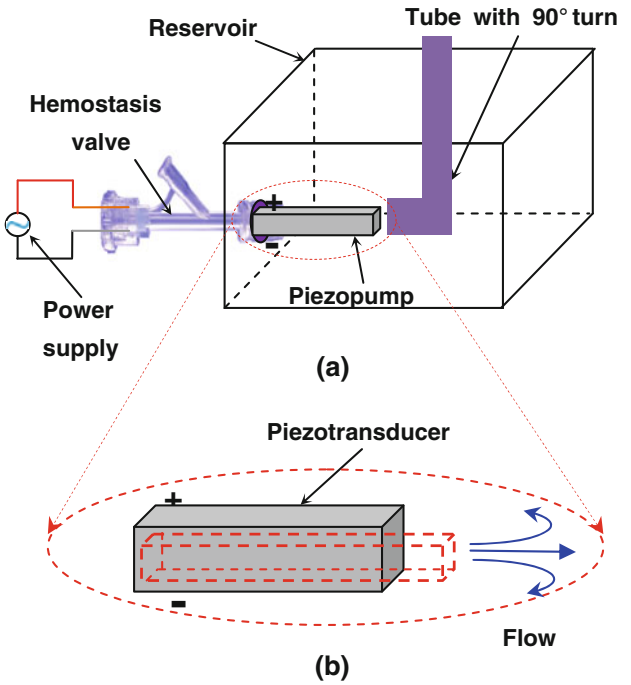

Fig. 2 Experimental setup for the flow experiment. **a** Schematic of test section. **b** Exaggerated view of the transducer

Fluoresbrite™ polychromatic red microspheres of 6 and 1 μm in diameter from Polysciences, Inc. with peak excitation and emission wavelengths of 491 and 554 nm, respectively, were used as tracer for flow visualization. Excitation of the fluorescent microspheres was accomplished using a 100 W High pressure mercury burner from Olympus Optical Company Ltd. The flow experiments setup was placed on an inverted microscope (Olympus IX 70). A Sensicam QE CCD camera (1376 × 1040 pixels) from Cooke Corporation was used to image the flow field with exposure times varying from 30 to 500 ms depending on the flow velocity. The camera was mounted on the microscope with objectives of 2.52× magnification.

The glass tube shown in Fig. 2a was used to quantify the pressure head and flow rate generated by the piezopump. Its horizontal part was also used to demonstrate the effect of the transducer tip's axial position relative to the tube end on pumping performance. The glass tube (both ends open) with ID of 1 mm and 90° turn on one end was placed, so that the end immersed in the liquid reservoir is quasi-coaxial to the piezoactuator. From energy equation (Fox and McDonald 1998), it can be concluded that the position of the free surface of the liquid in the vertical portion of this tube would be used to estimate pump pressure head Δp generated. In order to ensure that the 1 mm ID tube can be used to measure Δp accurately (accounting for both surface tension and viscosity effect), several different tubes with ID of 2.4, 3.4, and 4 mm, respectively, were also used to measure Δp as a function of AC frequency. The

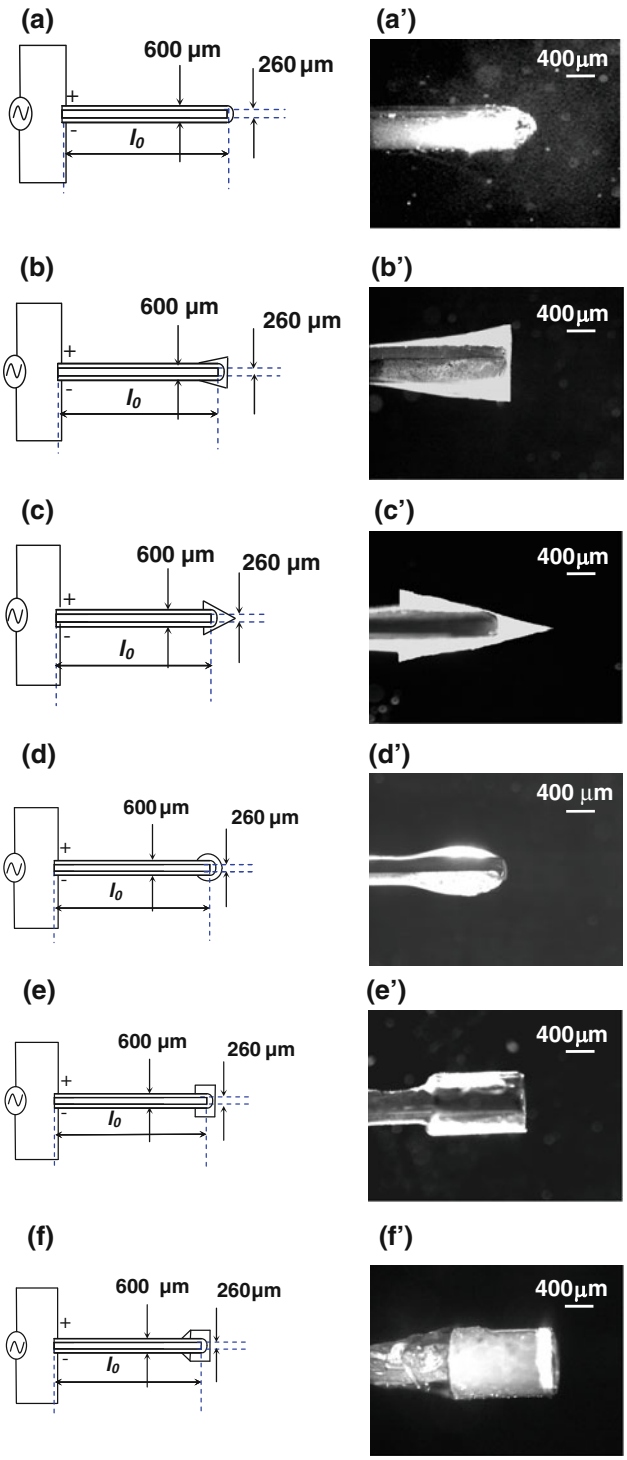

Fig. 3 **a**–**f** Different actuator tip configuration; **a′**–**f′** Microscopic images of the actual tip configuration obtained corresponding to **a**–**f** with 13.7× magnification (value of l_0 can be 30, 20, 14.4, and 10 mm)

consistency in results revealed that 1 mm ID tube can accurately predict the pressure head in this case. The results are presented in Sect. 4.2.3. All other measurements were then performed with 1 mm ID glass tube. The rate of

this height change was used as a measure of the pump flow rate Q which was calculated using the following equation (Sheen et al. 2008):

$$Q = \frac{\pi \times D^2}{4} \cdot \frac{\mathrm{d}h}{\mathrm{d}t} \tag{2}$$

where Q is the measured flow rate, D is the ID of the glass tube, and dh is the liquid level difference within a time interval dt.

Note that it has been assumed for ease of estimation that the hydrostatic pressure of the water column was at all times approximately equal to the pressure load on the pump.

3.2 Configuration of piezoactuator tip

Due to the gravity and capillary force of the complex coating fluid, the actuator tip became elliptical in shape after the coating as shown in Fig. 3a′ rather than perfectly flat as it was before the coating. We postulated that the shape of actuator tip might have an effect on flow velocity due to complicated solid–fluid interaction and the unidirectional nature of acoustic streaming. Hence, an attempt was taken to make different tip configuration of the same actuator to find out experimentally which one would give maximum flow velocity and eventually best pumping performance. Five other configurations were made and tested to find the best performance. Different configurations of the actuator tip are illustrated in Fig. 3a–f. Note that these figures are not drawn to scale. The length l_0 of all the transducers was selected as 30, 20, 14.4, and 10 mm, respectively. Configuration 3a is the actuator tip after coating (without any modification). Configuration 3b, c, and d were made under microscope using a glue. Configuration 3e was made by attaching a 1 mm length rigid microtubing with 690 μm ID and 840 μm outer diameter at the actuator tip. Configuration 3f has been made initially following the same procedure as 3e and then making the inner face (left side) blunt. The microscopic images of the actual tip configurations obtained are shown in Fig. 3a′–f′. All the images were taken with 13.7× magnification.

4 Experimental results and discussions

4.1 Flow visualization results

4.1.1 Acoustic streaming

We would consider first the case of fluid pumping capability of the piezotransducer in the absence of the glass tube. There is no vibration, and hence no acoustic streaming bulk flow without external electrical field as shown in Fig. 4a. Whereas an acoustic streaming and the resulting bulk fluid motion is generated as shown in Fig. 4b, when the piezotransducer is excited in d_{31} mode with an external electrical AC potential. In Fig. 4, microspheres are used as tracer. The camera exposure time was 50 ms. The field of view in Fig. 4 is 3.90 × 2.5 mm^2. The fluid near the actuator tip was observed in real-time, as it moves away from the actuator's tip face. It is clear from Fig. 4b that the flow direction was perpendicular to the transducer flat surface which is similar to the reported streaming induced by ultrasonic transducer. This strongly suggests that acoustic streaming (Riley 2001) results from the periodic disturbance, caused by the vibration of piezoactuator in this case. Figure 4 implies that actuation of piezotransducer in d_{31} mode can produce a pumping effect. The tip configuration in Fig. 4 corresponds to that in Fig. 3f′. Similar bulk fluid motion with different local streaming velocity was obtained for other actuator tip configurations as well which are not given here for brevity.

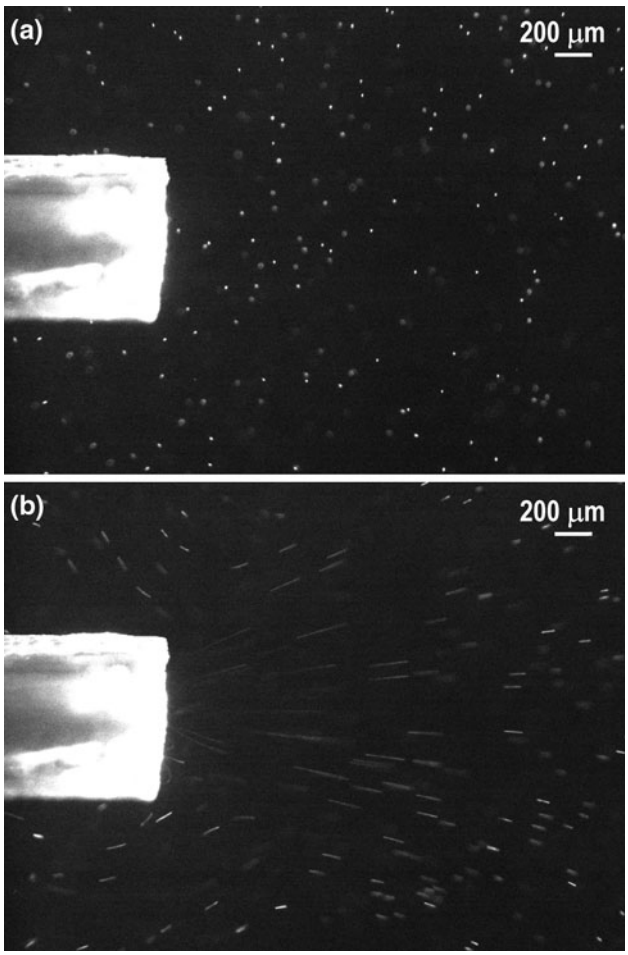

Fig. 4 Visualization of acoustic streaming caused by an oscillating piezoelectric transducer in d_{31} mode in water. **a** No vibration and there is no acoustic streaming bulk flow; **b** vibration with 58 $V_{P\text{-}P}$ at 41 kHz, The camera exposure time is 50 ms. The total area of the image is 3.90 × 2.50 mm^2

The applied electrical potential in Fig. 4b was 58 $V_{P\text{-}P}$ with a frequency of 41 kHz, which was supposed to be the resonant frequency of the piezoactuator as the maximum local velocity was observed at this frequency. The resonance frequency was determined from visualization results by varying frequency at a constant voltage. As the microspheres' streak length was proportional to the local velocity keeping the exposure time constant, the frequency corresponding to maximum streak length is expected to be the resonant frequency, which was determined from the un-aliased movie recorded by the camera. The reliability of this procedure can be proved by measuring the electrical admittance or impedance versus frequency curve of the piezoactuator. For this purpose, a Hewlett Packard 4194A Impedance Analyzer was used to measure the admittance of the transducer, as it was excited with various frequencies. The results were properly stored in a computer using Labview™ data acquisition program. The absolute value of experimental admittance (mhos) versus frequency (Hz) curve and the corresponding impedance versus frequency curve at constant applied voltage (58 $V_{P\text{-}P}$ in this case) is shown in Fig. 5a and b, respectively. The peak in admittance curve or the valley in impedance curve represents the resonance frequency, and according to Fig. 5, the resonance frequency was at 41.062 kHz which was almost in agreement with the flow visualization results obtained.

4.1.2 *Effect of actuator tip configuration on acoustic streaming*

As acoustic streaming is a unidirectional flow generated due to sound waves and arises from non-vanishing time averaged pressure and velocities generated by acoustic pressure when a sound field passes through (Nyborg 1998), the actuator tip might have an effect on the streaming velocity. Hence, the flow visualization experiments were performed for all configurations shown in Fig. 3a′–f′. Since power consumption is an important consideration in micropump application in many cases (e.g., microelectronics cooling), the piezotransducers with different tip configurations (but with nearly the same cross-sectional area and length) were excited at resonant frequency of each individual actuator design to obtain the maximum possible streaming velocity from that particular design for the same energy input. The input power is (0.32 W in this case) approximated by the following equation (Piezosystemjena 2009):

$$P_{\text{avg}} = C \cdot U_{\text{max}} \cdot V_{\text{P-P}} \cdot f \tag{3}$$

where P_{avg} is the average power in Watt, C represents the capacitance of piezotransducer (in Farad), $V_{P\text{-}P}$ is peak–peak drive voltage (in Volts), U_{max} is the maximum output voltage of the amplifier in Volts, and f denotes operating frequency in Hz.

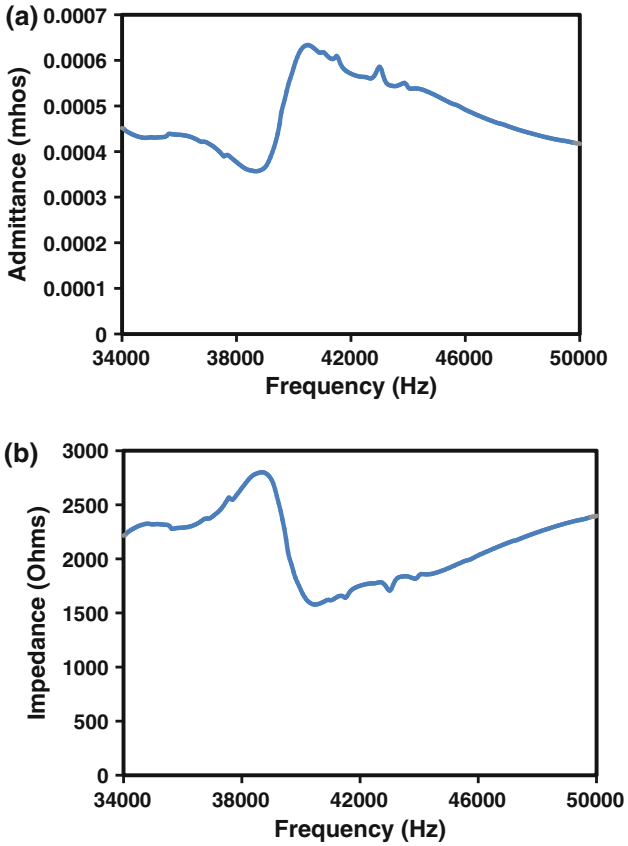

Fig. 5 Relationship of absolute value of admittance and impedance with AC frequency; **a** Relationship between absolute value of admittance and excitation frequency of piezotransducer. **b** Relationship between absolute value of impedance and excitation frequency of piezotransducer (the applied voltage was 58 $V_{P\text{-}P}$ in both cases)

The local velocity u near the actuator tip had been approximated as ratio of streak length and camera exposure time. The comparison of the maximum local velocities for different actuator tip configurations at constant electrical power input is presented in Fig. 6 where a′–f′ actually corresponds to the actuator tip configurations as shown in Fig. 3a′–f′, respectively. The maximum velocity u_{max} was measured near the same location (very close to the transducer surface) for all tip configurations. From the results, it is evident that configuration 3a′ gave u_{max} of 7 mm s^{-1}. Configuration 3b′, which has a trapezoidal tip configuration provided u_{max} of 8.5 mm s^{-1}. The triangular tip actuator (configuration 3c′) and the more elliptical tip (configuration 3d′) come up with u_{max} of 5.3 and 6.2 mm s^{-1}, respectively. Configuration 3e′ with flat tip provided a higher u_{max} of 11 mm s^{-1} than the previous configurations. Finally, configuration 3f′ showed that the best result with u_{max} of 13.5 mm s^{-1} when the tip was flat, and the inner face was blunt. The worst results were obtained for the configuration 3c′. As the tip configurations had been made manually, three actuators with identical tip configuration

were made and tested under the same conditions to evaluate the reliability of the results aforementioned. The results come up with an experimental uncertainty of only 1 mm s^{-1} for all the configurations as illustrated using a vertical error bar in Fig. 6. The orders of magnitude of u_{max} for different configurations remained the same.

The effect of tip configuration on streaming pattern is interesting and yet complicated. A simplified explanation of shape effect based on directed body force acting on the fluid exerted by the piezoelectric transducer is proposed. In this study, the net flow expected is in the positive x-direction. We propose an illustrative and qualitative explanation depending on the net acoustic streaming force acting in x-direction in the absence of glass tube. Let us imagine each point on transducer tip as a source of acoustic streaming force.

Assume that the force acts perpendicular to the surface on the transducer tip can generate the streaming and that the acoustic streaming observed is generated by the component of the force in x-direction, not the force component in y-direction. The variation of x-component of this force is most likely responsible for variation of u_{max} with tip configurations. For simplification, the tip surface is divided into several sub-regions (as shown by colored dotted lines in Fig. 7) and the imaginary resultant force emitting from each sub-region has been shown as a point force perpendicular to that surface.

Figure 7a–f corresponds to the tip configuration as shown in Fig. 3a′–f′. Let us consider the configuration 7d to give a qualitative explanation of the shape effect. For Fig. 7d, the effective force emitting from the transducer tip in x-direction F_x can be written as:

$$F_x \sim F_1 + F_2\cos\alpha_1 + F_3\cos\beta_1 + F_4\cos 90^\circ - F_5\cos 90^\circ - F_6\cos\alpha_2 - F_7\cos\beta_2. \quad (4)$$

Here F_1, F_2, F_3, F_4, F_5, F_6, and F_7 are the resultant forces in the sub-regions and α_1, β_1, α_2, and β_2 are the angles with the positive x-axis or negative x-axis, respectively as shown in the Fig. 7d. Similarly, we can derive the effective force in x-direction for all other configurations.

If we carefully examine the net force expression in x-direction, much larger value of F_1 for the cases of Fig. 7b, e, and f (due to the larger flat area associated with F_1) possibly make them superior to other three (7a, c, and d) which has been confirmed in the experiments (see Fig. 6), since the total acoustic streaming force is mainly distributed in the x-direction.

Comparing Figs. 7a, c, and d, force contribution from F_1 is the smallest for 7c compared to 7a and d as the projection area associated with this force is the smallest for 7c. The values of α_1 and β_1 being higher than the other two, results in the components of F_2 and F_3 to be smaller for 7c in positive x-direction and the negative contribution of F_8 and F_9 further reduce the net force F_x. For 7d, the contribution of F_1 is larger than 7c and a. However, the contribution from F_6 and F_7 in opposite direction results in reduction of the streaming velocity in positive x-direction compared with the case of Fig. 7a, but still better than 7c

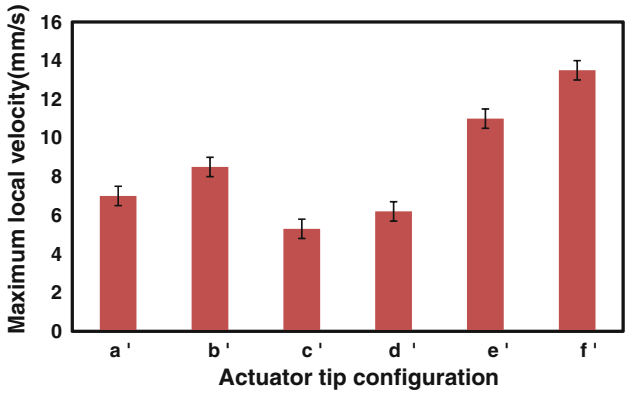

Fig. 6 Effect of actuator tip configuration on the maximum local streaming velocity (at constant P_{avg})

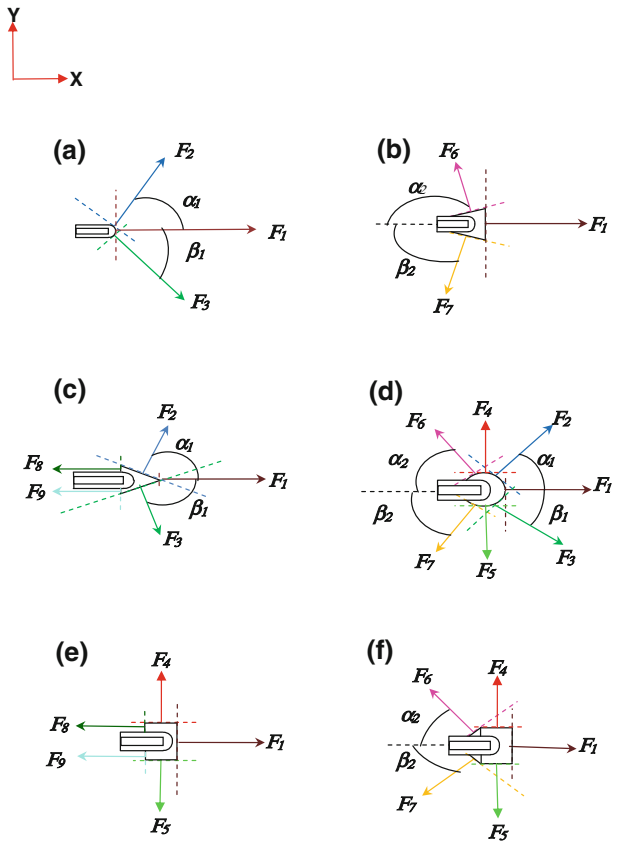

Fig. 7 Force analysis of tip configuration affecting the streaming velocity (for explanation, see the text)

due to the larger contribution of F_1 and lower negative effects of F_6 and F_7 compared to F_8 and F_9 in the case of 7c.

Much larger contribution of F_1 due to larger flat area causes the other three (Figs. 7b, e, and f) to give higher u_{max}, since more acoustic streaming force is distributed in the flat area. For 7b, the contribution of F_1 is relatively large. However, the negative contribution from F_6 and F_7 cannot make it better than 7e and f. Although, it appears that the negative contribution of F_8 and F_9 in the case of 7e should be larger than that of F_6 and F_7 of 7b, the net force in the case of 7e is found to be more as u_{max} from 7e is higher than that of 7b (see Fig. 6). This may be due to smaller projection area associated with F_8 and F_9 in the case of 7e.

The reason why 7f gives the highest u_{max} is that the contribution of F_1 is the same as 7e, but the negative contribution from F_6 and F_7 is much less compared to F_8 and F_9 in case of 7e due to larger values of α_2 and β_2.

However, effect of tip configuration is complicated and requires further study. Note that several effects have not been considered here, e.g., the effect of shape on the transverse dimension of the acoustic field which primarily depends on size of transducer and secondarily on diffraction. Complete understanding of the effect of tip configuration requires detailed flow field and pressure field investigation, e.g., through micro-PIV.

The velocity magnitudes of the streaming should depend on the applied electrical voltage, AC frequency, and original length of actuator, actuator material properties, electrode separation distance, and working fluid. In the following section, we will quantify the pumping characteristics for the best actuator tip configuration as shown in Fig. 3f′. We will show the induced pressure head as a function of the actuator tip position along the tube length, applied electrical voltage, AC frequency, and length of actuator.

4.2 Pressure head results

In Figs. 8, 9, 10, 11, 12, 13, and 14, the curves presented are composed of data points which are averages of three realizations, and are for the actuator tip configuration of Fig. 3f′. All measurements were reproducible. The experimental uncertainty in each case is shown by a vertical error bar. Since the working fluid is DI water, the pressure head results are approximated in terms of mm of H_2O unit.

4.2.1 Pressure head as a function of axial position of actuator tip

The pressure head Δp induced by the pump was found to be sensitive of the axial position of actuator tip near the left end of the tube ($x/D = 0$) within a range of $|x|/D < 1.5$, where D is the tube ID and x is the axial position of piezoactuator tip. This is shown in Fig. 8, where the actuator

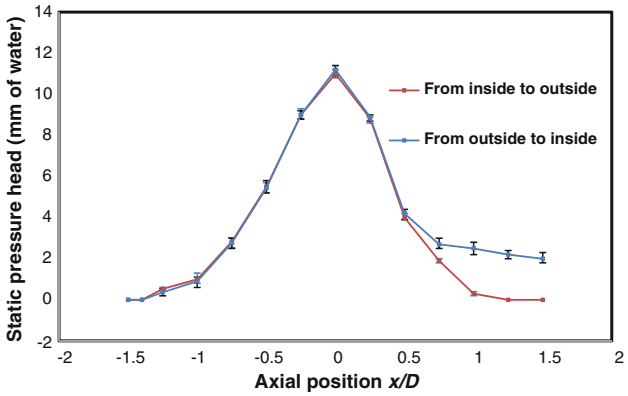

Fig. 8 Relationship between Δp and axial position of the actuator tip along the tube axis (the electrical voltage was 75 $V_{P\text{-}P}$ and excitation frequency 41 kHz)

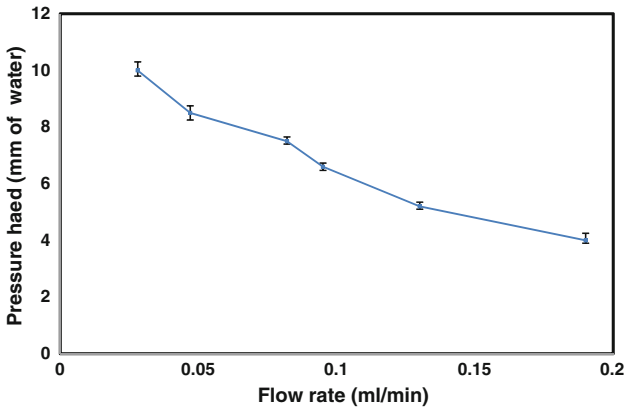

Fig. 9 Relationship between pressure head and flow rate at $x/D = 0$ with voltage = 75 $V_{P\text{-}P}$ and $f = 41$ kHz

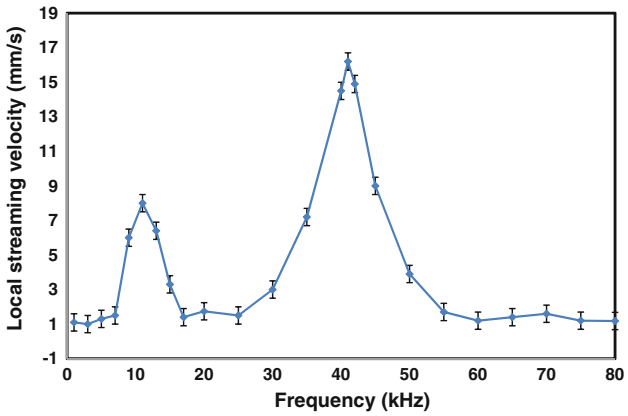

Fig. 10 Variation of local streaming velocity with frequency at constant voltage (75$V_{P\text{-}P}$)

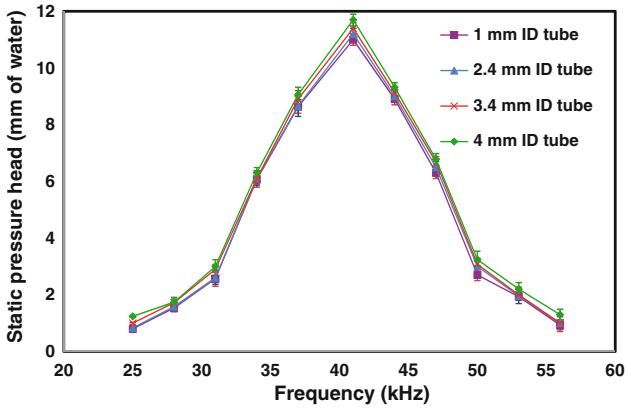

Fig. 11 Effect of frequency on static pressure head generated at constant voltage (75 $V_{P\text{-}P}$)

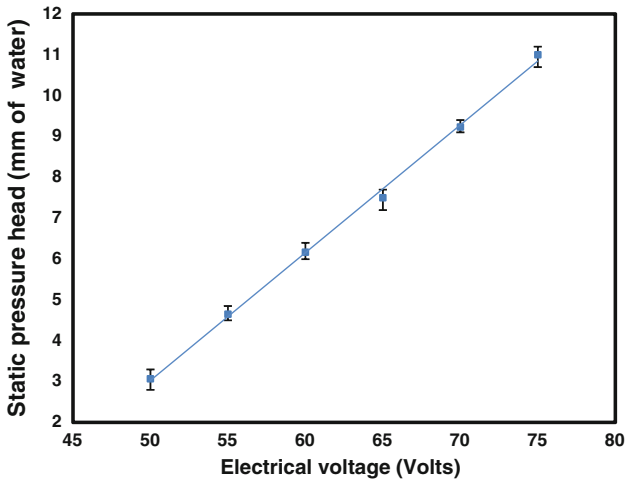

Fig. 12 Distribution of static pressure head with variation of voltage at constant frequency (41 kHz)

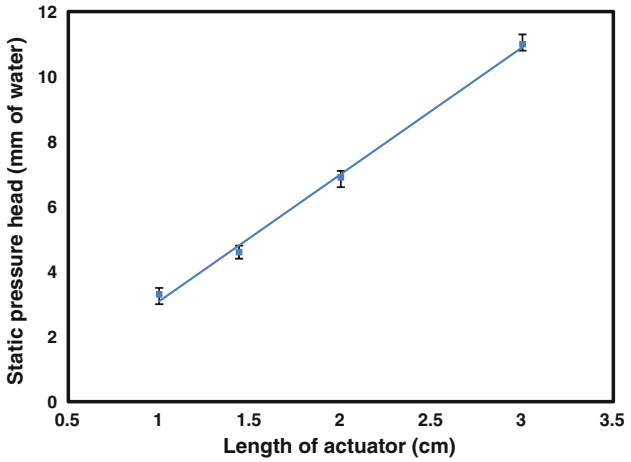

Fig. 13 Dependence of generated static pressure head on length of actuator at constant voltage (75 $V_{P\text{-}P}$)

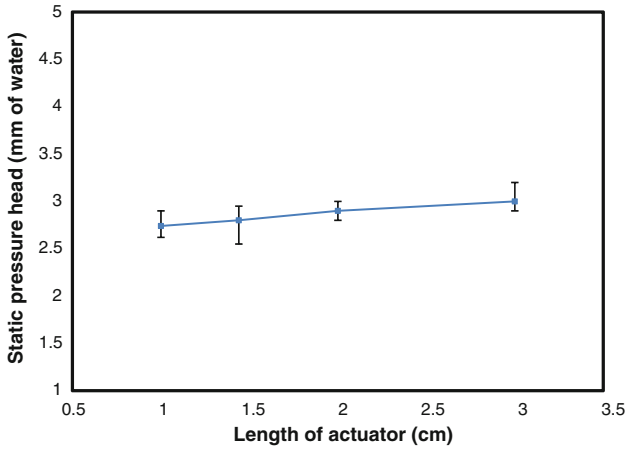

Fig. 14 Effect of length of actuator on static pressure head generated at constant electrical power input

was placed along the tube axis with AC voltage $V = 75$ $V_{P\text{-}P}$, frequency $f = 41$ kHz. The negative x-coordinate in Fig. 8 corresponds to positions where the actuator tip was placed outside the left end of the tube. Initially, the actuator tip was placed inside the tube at $x/D = 1.75$ with no measurable pressure rise. The pressure rise was zero until x/D decreased to a value of $x/D = 1$. Further translation of the actuator tip resulted in an increase in Δp to a maximum value of 11 mm of H_2O at $x/D = 0$. As the actuator tip was further moved away from the left end of the tube to negative values of x/D, Δp rapidly decreased again until $x/D = -1.4$ where Δp was nearly zero. With further movement of the actuator to left, Δp remained zero. For these measurements, the experimental uncertainty value is shown by a vertical error bar for all data points which varies from 0.2 to 0.5 mm.

Another interesting phenomenon is observed that Δp was not only a function of x but also a function of the history of the tip position. This is demonstrated as a second experimental curve in Fig. 8, where the actuator tip was moved from $x/D = -1.5$ toward higher values of x/D. For this direction of translation, when x/D was equal to 1.5, Δp was approximately 2 mm of H_2O (compared to the zero values measured before). This behavior implies that there was a hysteresis for the flow behavior associated with the pumping. The signal was turned off, when the tip was moved in or out of the tube, and the rate of translation of actuator tip was kept extremely slow (in the order of 0.01 mm/s). At each position, where Δp was read, the translation stage was at rest for a sufficiently long time, so that Δp became stable for measurement.

Irrespective of this hysteresis, Fig. 8 shows that Δp is much higher just at the tube end than either inside or outside the tube, and Δp produced is a strong function of x/D. Each point in Fig. 8 reflects a steady-state Δp value achieved by the pump at each position. These experimental results follow almost the similar trend observed by Wang et al. (2004) to characterize their laser-induced cavitation pump.

4.2.2 Relationship between pressure head and flow rate

In the next sections, we would present only measurements of Δp at $x/D = 0$. Figure 9 shows the relationship between Δp and flow rate Q, for $V = 75$ $V_{P\text{-}P}$ and $f = 41$ kHz. The measurements show that Δp decreases with increasing Q. This matches the typical characteristic curve of fluid pump performance as illustrated by White (1994), although an ideal linear dependence of Q on Δp was not observed. At Δp of 4 mm of H_2O, Q is found to be 0.2 ml/min. The experimental uncertainty for these data points fall between 0.35 and 0.5 mm which is shown in the Fig. 9 with a vertical error bar. Higher flow rate can be achieved through improved designs with multiple pumps in parallel. Conversely, larger pressure head can be gained by arranging multiple pumps in series.

4.2.3 Distribution of pressure head with variation of frequency

The variation of u with change of frequency at constant voltage is illustrated in Fig. 10, where two peaks of local velocities were achieved, one at lower end (11 kHz) of frequency spectrum and the other at higher end (41 kHz). Comparison of the two peaks implies that operation of the micropump at higher peak would give better performance as the value of u at higher peak is greater than that at the lower peak. Note that this variation of u as a function of f actually reflects a strong relationship between impedance of the device and f. u_{max} corresponds to the f where admittance is maximum or impedance is minimum (see Fig. 5). Hence, the Δp versus f curve is obtained only at higher frequency spectrum (20–60 kHz).

Figure 11 displays the relationship between static pressure head Δp and AC frequency f at a constant electrical potential (75 $V_{P\text{-}P}$) within a frequency range of 25–56 kHz. The experiment was performed with different ID (1, 2.4, 3.4, and 4 mm) glass tube to observe the effect of surface tension and viscosity on measurements. The results demonstrate that 1 mm ID tube was able to correctly predict the pressure head in this case. The curves obtained (shown in Fig. 11) with different ID tube are consistent to one another, and show a similar trend over the frequency range. Experimentally, Δp was found to be sensitive to f. No measurable pressure rise was observed at a frequency <25 kHz and >56 kHz. An increase in Δp along with an increase in f was observed starting from 25 kHz up to 41 kHz, where it reached a maximum value of 11 mm of H_2O. For $f = 41$ kHz, where Δp reaches maximum, the maximum absolute error is 0.7 mm, and maximum relative error is approximately 6%. Further increase in f led to a decrease in Δp and this trend continues until Δp reaches a zero value at $f \geq 56$ kHz.

These experimental results are quite similar in trend with those obtained by Lima et al. (2009) in characterizing their biomimetic piezoelectric pump developed using bimorph actuator. This behavior indicates a guideline that this type of pumping device should be operated at optimal frequency to obtain higher Δp. Finally, the experimental uncertainty for all these data points stay between 0.1 and 0.6 mm.

Note that attention has to be paid to the operation under resonance frequency. When a piezotransducer is operated at resonance frequency under mechanical loading, it can be damaged. Therefore, it should usually be avoided to operate the piezotransducer at resonance frequency. However, for the micropump case, the mechanical load is relatively small, and vibrating fluid should not cause damage of the transducer when the supplied voltage is not very high.

4.2.4 Effect of electrical voltage (V) on static pressure head (Δp)

The dependency of Δp on the V at constant f (41 kHz) is shown in Fig. 12. V was varied from 50 to 75 $V_{P\text{-}P}$ with an increment of 5 V. It is evident from the figure that as V was increased, Δp also increased. The relationship between Δp and V was quite linear. The linear relationship can be explained with the use of Eq. 1. Provided the other parameters remain constant, the amplitude of displacement is proportional to voltage only. We assume that the acoustic streaming velocity is linearly proportional to the displacement, the corresponding Δp should thus be linearly related to V. (Similar relation has been also observed in the case of bimorph piezoelectric actuator pump, where generally the static pressure head generated by the piezoelectrically actuated pump depends directly on the amplitude of actuator tip displacement (Lima et al. 2009)). Hence, Δp increases linearly as the voltage increases at a constant f.

4.2.5 Actuator length effect on pumping performance

In order to evaluate the effect of the actuator's length l_0 on the pumping performance, four different lengths with the same cross-sectional area were tested. l_0 was varied from 10 to 30 mm. The relationship between Δp and l_0 at constant V (75 $V_{P\text{-}P}$) is displayed in Fig. 13. As l_0 decreased from 30 to 10 mm, Δp also decreased almost linearly. This behavior can be explained on the basis of the Eq. 1 as well. It is evident from the equation that the amplitude of the displacement is proportional to l_0 only when other variables (D_f, V, and d_{31}) stay constant. Therefore, Δp shows linear decrease in value in response to the decrease of the length of actuator.

Note that to investigate l_o effect on Δp completely, we also need to keep constant P_{avg}. However, according to Eq. 3, P_{avg} depends on the C of the piezotransducer, which, in turn, is related to the transducer's length l_o. The change of l_o will also change the resonance frequency of the

Table 1 Measured relationship among the transducer length, capacitance, AC frequency (corresponding to the resonance frequency), and AC voltage for a given electrical power input

l_0 (cm)	C (pF)	f (kHz)	V (volts)	P_{avg} (Watt)
3	1,245	41	50	0.36
2	526	53	91.5	0.36
1.44	320	67	119.8	0.36
1	247	73	141.2	0.36

transducer. Thus, to maintain constant P_{avg} for different l_o, V has to be adjusted at the AC frequency, which corresponds to the resonance frequency. The corresponding values are shown in Table 1. Figure 14 illustrates the relationship between Δp and l_o at constant P_{avg} instead of constant V as shown in Fig. 13. The results indicate an interesting phenomenon that there was no significant difference in Δp along with the change of l_0 at constant P_{avg}, although a small decreasing trend was observed with decrease in length of actuator. These results provide a good indication of the probability of further miniaturization.

5 Future works and improvements

There are several scopes of improvement and future works to understand completely the dynamic micropumping phenomena demonstrated in this study. Unveiling the detailed flow field near the actuator tip and the tube by micro particle image velocimetry (μ-PIV) for different tip configurations can provide fundamental understanding of the dynamic micropumping phenomenon and thus help to aid the design of a better pump. The effect of transducer diameter (varying both the thickness of coating and cross-section of the transducer separately) on pumping performance will improve the parametric study. The actual displacement of the tip at operational frequency range would be another interesting study. This can be accomplished using a laser Doppler interferometer or optic fiber sensor. Alternatively, an optical measurement system can be setup to measure the displacement. In order to achieve higher flow rate multiple pumps can be arranged in parallel, whereas pressure can be presumably increased by arranging multiple pumps in series.

6 Conclusions

We have presented the experimental characterization of a novel valveless micropumping phenomenon using a single piezotransducer actuated in d_{31} mode. The actuator tip configuration has significant effect on the pumping performance. Influence on the pressure head generated by the pump from parameters, such as AC frequency, voltage, position of the actuator tip, and the length of the actuator have been experimentally investigated. For the flow pumping phenomenon demonstrated, a relationship between flow rate and pressure head is drawn which is identical to a typical fluid pump. The pumping performance, i.e., static pressure head is found to be sensitive to both applied electrical voltage and excitation frequency. The relationship between static pressure head and applied electrical voltage is quiet linear for a certain excitation frequency. On the other hand, best result for static pressure head is obtained when the piezotransducer is excited at resonant frequency. This can be an important consideration for designers of fluidic devices. Dependence between static pressure head and length of actuator is linear as well. The presented pumping phenomenon has the potential to provide a low cost, compact, simple, and more reliable micropump in microfluidics application.

Acknowledgments This study has been partially supported by the ONR (Office of Naval Research under ESRDC consortium) and partially by NSF RII funding (EPS-0447660). Discussion with Mr. Thomas Daue from Smart Material Corp. is appreciated. Special thanks to Fazle Rabbi, Monjur Morshed, and Raihan Rassel for discussion and revising this article.

References

Acikalin T, Wait S, Garimella S, Raman A (2004) Experimental investigation of the thermal performance of piezoelectric fans. Heat Transf Eng 25(1):4–14

Ahn C, Allen M (1995) Fluid micropumps based on rotary magnetic actuators. Proceedings of IEEE Micro Electro Mechanical Systems (MEMS), Amsterdam, pp 408–412

Askeland DR, Phule PP (2006) The science and engineering of materials, 5th edn. Thomson, New York, USA

Basak S, Raman A, Garimella S (2005) Dynamic response optimization of piezoelectrically excited thin resonant beams. J Vibr Acoust 127(1):18–27

Beebe DJ, Mensing GA, Walker GM (2002) Physics and applications of microfluidics in Biology. Annu Rev Biomed Eng 4:261–286

Bourouina T, Bosseboeuf A, Grandchamp JP (1997) Design and simulation of an electrostatic micropump for drug-delivery applications. J Micromech Microeng 7:186–188

Cui Q, Liu C, Zha XF (2007) Study on a piezoelectric micropump for the controlled drug delivery system. Microfluid Nanofluid 3:377–390

Du XY, Swanwick ME, Fu YQ, Luo JK, Flewitt AJ, Lee DS, Maeng S, Milne WI (2009) Surface acoustic wave induced streaming and pumping in 128° y-cut $LiNbO_3$ for microfluidic applications. J Micromech Microeng 19. doi:10.1088/0960-1317/19/3/035016

Fox RW, McDonald AT (1998) Introduction to fluid mechanics. Wiley, New York

Garimella SV, Singhal V, Liu D (2006) On-Chip thermal management with microchannel heat sinks and integrated micropumps. Proc IEEE 8:1534–1548

Gerlach T, Schuenemann M, Wurmus H (1995) A new micropump principle of the reciprocating type using pyramidic micro flow-channels as passive valves. J Micromech Microeng 5:199–201

Gong QL, Zhou ZY, Yang YH, Wang XH (2000) Design, optimization and simulation on microelectromagnetic pump. Sens Actuat A 83:200–207

Hashimoto K, Ikekame K, Yamaguchi M (1997) Micro-actuators employing acoustic streaming caused by high-frequency ultrasonic waves. Transducers '97, pp 805–808

Iverson BD, Garimella SV (2008) Recent advances in microscale pumping technologies: a review and evaluation. Microfluid Nanofluid 5:145–174

Jeong OC, Yang SS (2000) Fabrication and test of a thermopneumatic micropump with a corrugated p plus diaphragm. Sens Actuat A 83:249–255

Kan J, Tang K, Liu G, Zhu G, Shao C (2008) Development of serial-connection piezoelectric pumps. Sens Actuat A 144:321–327

Kim Y, Wereley S, Chun C (2004) Phase-resolved flow field produced by a vibrating cantilever plate between two endplates. Phys Fluids 16(1):145–162

Koch M, Harris N, Evans A, White N, Brunnschweiler A (1998a) A novel micromachined pump based on thick-film piezoelectric actuation. Sens Actuat A 70:98–103

Koch M, Evans AGR, Brunnschweiler A (1998b) The dynamic micropump driven with a screen printed PZT actuator. J Micromech Microeng 8:119–122

Laser DJ, Santiago JG (2004) A review of micropumps. J Micromech Microeng 14:35–64

Lima CRD, Vatanabe SL, Choi A, Nakasone PH, Pires RF, Silva ECR (2009) A biomimetic piezoelectric pump: computational and experimental characterization. Sens Actuat A 152:110–118

Loh BG, Hyun S, Ro PI, Kleinstreuer C (2002) Acoustic streaming induced by ultrasonic flexural vibrations and associated enhancement of convective heat transfer. J Acoust Soc Am 111(2): 875–883

Ma B, Liu S, Gan Z, Guojun L, Cai X, Honghai Z, Yang Z (2006) A PZT insulin pump integrated with a silicon microneedle array for transdermal drug delivery. Microfluid Nanofluid 2:417–423

Nguyen NT, White RM (1999) Design and optimization of an ultrasonic flexural plate wave micropump using numerical simulation. Sens Actuat A 77:229–236

Nyborg WL (1998) Acoustic streaming, nonlinear acoustics. Academic press, New York, pp 207–231

Piezosystemjena (2009) Piezoline. http://www.piezojena.com/files.php4?dl_mg_id=229&file=dl_mg_1195142143.pdf

Reyes DR, Iossifidis D, Auroux P, Manz A (2002) Micro total analysis systems. 1. Introduction, theory and technology. Anal Chem 74:2623–2636

Rife J, Bell M, Horwitz J, Kabler M, Auyeung R, Kim W (2000) Miniature valveless ultrasonic pumps and mixers. Sens Actuat A 86:135–140

Riley N (2001) Steady streaming. Ann Rev Fluid Mech 33:43–65

Ryu WH, Huang Z, Prinz BF, Goodman SB, Fasching R (2007) Biodegradable micro-osmotic pump for long-term and controlled release of basic fibroblast growth factor. J Control Release 124:98–105

Sheen HJ, Hsu CJ, Wu TH, Chang CC, Chu HC, Yang CY, Lei U (2008) Unsteady flow behaviors in an obstacle-type valveless micropump by micro-PIV. Microfluid Nanofluid 4:331–342

Singhal V, Garimella SV, Raman A (2004) Microscale pumping technologies for microchannel cooling systems. Appl Mech Rev 57:191–221

Tsai JH, Lin L (2002) Active microfludic mixer and gas bubble filter driven thermal bubble micropump. Sens Actuat A 97–98: 665–671

Ullman A, Fono I, Taitel Y (2001) A piezoelectric valve-less pump-dynamic model. J Fluid Eng 123(1):92–98

Wang GR, Santiago JG, Mungal MG, Young B, Papademetriou S (2004) A laser induced cavitation pump. J Micromech Microeng 14:1037–1046

White FM (1994) Fluid mechanics, 3rd edn. McGraw Hill Inc., New York

Woias P (2005) Micropumps—past, progress and future prospects. Sens Actuat B 105:28–38

Zhang L, Koo JM, Jiang L, Asheghi M, Goodson KE, Santiago JG, Kenny TW (2002) Measurements and modeling of two-phase flow in microchannels with nearly constant heat flux boundary conditions. J Microelectromech Syst 11:12–19

Zhang C, Xing D, Li Y (2007) Micropumps, microvalves, and micromixers within PCR microfluidic chips: advances and trends. Biotechnol Adv 25:483–514